RSC Advances

PAPER

View Article Online
View Journal | View Issue

Cite this: *RSC Adv.*, 2023, **13**, 30168

Phosphorus-substitution effect on the phase stabilization, electrical and spectroscopic properties of LAMOX-based electrolyte for solid oxide fuel cells

Noureddine Mhadhbi,[ab] Wiem Jabeur,[a] Ahlem Guesmi,[c] Ammar Houas,[d] Naoufel Ben Hamadi[c] and Houcine Naïli *[a]

Received 16th July 2023
Accepted 9th October 2023

DOI: 10.1039/d3ra04777f

rsc.li/rsc-advances

A series of P^{5+} – doped $La_2Mo_2O_9$ phases with different concentrations of P^{5+} were prepared using conventional solid–state reactions. The formation of phase-pure P^{5+}-doped $La_2Mo_2O_9$ has been monitored by powder X-ray diffraction, thermal analysis, conductivity measurements, Raman, and FT-IR absorption techniques. The structure and lattice parameters of $La_2Mo_{2-y}P_yO_{9-y/2}$ are obtained from Rietveld refinement. The effect of substituting P for Mo reveals that the phase transition which occurs in $La_2Mo_2O_9$ around 560 °C disappears when $y > 0.02$, as demonstrated by thermal analysis. Pure P^{5+}-doped phases with monoclinic structure (α-form, the space group $P2_1$) were observed for the concentration of optically active ions up to $y = 0.02$. When the concentration of P^{5+} ions is higher, a cubic structure (β-form, the space group $P2_13$) starts to appear. However, up to the concentration of $y = 0.03$ of the P^{5+} ion a mixture of the monoclinic and cubic phases has been observed. From infrared and Raman analysis it is confirmed that different vibration modes arise from the vibration of molybdenum–oxygen bands. Mo–O bond lengths are also found to be independent of P-doping.

1. Introduction

There is currently considerable interest in finding competitive electrolytes to substitute the reference material yttria-stabilized zirconia (YSZ) in solid oxide fuel cell (SOFC). However, this electrolyte must be operated at 800–1000 °C to provide sufficient ionic conductivity. Such a high operating temperature limits the commercialization of SOFCs. Considerable effort has been exerted to develop alternative electrolytes possessing high ionic conductivities at intermediate temperatures (500–700 °C).[1,2] $La_2Mo_2O_9$ based materials (LAMOX) have been studied in last few years as potential solid electrolytes for intermediate temperature applications, such as oxygen sensor, dense membranes for oxygen separation and electrolyte for solid oxide fuel cells (SOFCs).[3] The attention has moved to electrolytes based on the lone pair substitution (LPS) concept. A partial or complete substitution of the lone pair cation by a non-lone pair cation produces intrinsic oxygen vacancies. This concept was first discovered by P. Lacorre *et al.* in the year 2000.[4,5] At around 580 °C, $La_2Mo_2O_9$ goes through a structural phase transition from the low-temperature α-$La_2Mo_2O_9$ monoclinic phase to the high-temperature β-$La_2Mo_2O_9$ cubic phase accompanied by two orders of magnitude increase in conductivity.[6–8] It has recently been reported that this phase transition is understood as a transformation from a static to a dynamic distribution of oxygen defects[7,9,10] while keeping the monoclinic local structure.[7] This phase transition is accompanied by a sudden increase of conductivity at higher temperatures that achieves about 6×10^{-2} s cm^{-1} at 800 °C, limiting the potential applicability of $La_2Mo_2O_9$ in SOFC. The current focus is on the stabilization of the intensely conducting β-phase. In this context, several series of compounds derived from $La_2Mo_2O_9$, designated as LAMOX, have been investigated in the past several years, in which La^{3+}, has been partially substituted by Ca^{2+}, Gd^{3+}, Y^{3+}, K^+, Sr^{2+}, Ba^{2+}, Bi^{3+}, and Eu^{3+} and Mo^{6+} by Nb^{5+}, Ta^{5+}, Re^{6+}, V^{5+}, Cr^{6+}, W^{6+} and S^{6+}.[11–18] In most cases, the β phase is stabilized to room temperature and the α/β phase transition is suppressed. Unfortunately, most of the substitutions decrease the conductivity at high temperatures in comparison with pure $La_2Mo_2O_9$. Vastly researchers have reported different applications resulting from the use of the LAMOX family in various fields[19–24] to achieve cell function success. This is due to several factors including the starting materials, the substituted

[a]*Laboratory Physico Chemistry of the Solid State, Department of Chemistry, Faculty of Sciences, University of Sfax, BP 1171, Sfax 3000, Tunisia. E-mail: houcine.naili@fss.rnu.tn*

[b]*University of Monastir, Preparatory Institute for Engineering Studies of Monastir, Monastir 5019, Tunisia*

[c]*Chemistry Department, College of Science, IMSIU (Imam Mohammad Ibn Saud Islamic University), P.O. Box 5701, Riyadh 11432, Saudi Arabia*

[d]*Research Laboratory of Catalysis and Materials for Environment and Processes, University of Gabes, City Riadh Zerig, Gabes 6029, Tunisia*

element, and the type of atmospheric conditions used during the synthesis process.[18] It is crucial to better understand how a substitution impacts the local patterns and the resulting material properties. LAMOX with molybdenum substituted by phosphorus is an example of a cationic substitution system in which saturation occurs at low concentrations as proved by Pahari *et al.*, since 2012.[25] The motivation for the present investigation was at first to determine the extent of the solid solution and then to obtain a better insight into the influence of phosphorus on the crystal structure, the thermal stability and the electrical properties. Also a correlation between the structural and ion conduction results has been established. From infrared and Raman analysis it is confirmed that different vibration modes arise from the vibration of molybdenum–oxygen bands. Mo–O bond lengths are also found to be independent of P-doping.

2. Materials and methods

Two grams of polycrystalline samples of $La_2Mo_{2-y}PyO_{9-y/2}$ ($y = 0.01, 0.02, 0.03, 0.04, 0.05$) were prepared by conventional solid–state reaction from elementary oxides molybdenum trioxide MoO_3 (PURA-TREMs 99.999% from Strem Chemicals), diammonium hydrogenphosphate $(NH_4)_2HPO_4$ (≥98% from Sigma Aldrich), and of lanthanum oxide La_2O_3 (reaction 99.9% from Alfa Aesar). The reaction between the reactants powders is written as follows:

$$La_2O_3 + (2 - y)MoO_3 + y(NH_4)_2HPO_4 \rightarrow La_2Mo_{2-y}P_yO_{9-y/2} + 2yNH_3 + 1.5yH_2O$$

Before use, La_2O_3 was calcinated in the air for 12 h at 1000 °C to remove absorbed carbon dioxide. The stœchiometric mixture of La_2O_3, $(NH_4)_2HPO_4$, and MoO_3 was first heated at 500 °C for 12 h (heating and cooling rates of 5 °C min^{-1}). Several annealing with regrinding in acetone is necessary to obtain a pure single phase. The final firing temperatures were 900, 950, 1000, 1100, 1150, and 1175 °C (heating and cooling rates of 5 °C min^{-1}) for phosphorus content lower and higher than $y = 0.03$, respectively.

After completion, X-ray powder diffraction patterns were recorded at room temperature on a θ/θ Bragg–Brentano Philips X'pert MPD PRO diffractometer ($CuK\alpha_{1+2}$ radiations) equipped with the X'celerator detector. At room temperature, diffractograms were collected for 400 min in the [5–130°] scattering angle range, with a 0.084° step. Thermodiffractograms were collected on the same diffractometer equipped with an HTK 1200 Anton Paar chamber using an Al_2O_3 sample holder cup. Diffractograms were recorded under air flow from room temperature (RT) to 900 °C in the [9–130°] scattering angle range, with a 0.0084° step (heating rate of 10 °C min^{-1}, temperature stabilization for 20 min with temperature correction after calibration). Crystal cell parameters were determined by full pattern matching refinement of the powder XRD patterns in space group $P2_13$ using the Fullprof program and the Diamond software was used to draw the crystal structure.[26]

Thermal analyses were performed on raw powders with a TGA/DTA Q600 SDT TA Instruments apparatus (Pt crucibles, Al_2O_3 as a reference) under airflow (100 mL min^{-1}). For numerous compounds in powder form in $La_2Mo_{2-y}PyO_{9-y/2}$ series, thermograms were collected on ~100 mg samples in the RT-1400 °C range heating/cooling rate of 10 °C min^{-1}.

Complex impedance measurements were performed on dense pellets, with thin platinum films (deposited by magnetron sputtering on both flat faces) as electrodes. The impedance spectra were recorded over the 32 MHz to 0.1 Hz frequency range (signal amplitude 50 mV) in dry airflow at high temperature using a Solartron SI 1260 frequency response analyzer combined with the Dielectric Interface (Solartron 1296). A 35 min thermalization time was applied before each measurement.

3. Results and discussion

3.1. XRD and thermal analysis

XRD patterns for different compositions of $La_2Mo_{2-y}P_yO_{9-y/2}$ at room temperature are shown in Fig. 1. The sharp and well-defined diffraction patterns indicate high range order of crystallinity. The unit cell parameters were obtained by the pattern-matching fit of diffractograms either in a single monoclinic subcell (space group $P2_1$ (no. 4)) for $y = 0.02$ or in a cubic cell (space group $P2_13$ (no. 298)) for $y = 0.03$. Along the series, the linear reduction of the unit cell volume with increasing the phosphorus content y reflect that the pentavalent phosphorus cation (ionic radii = 0.38 Å) is much smaller than molybdenum ion (ionic radii = 0.65 Å). The formation of a partial solid solution is then established in the composition range with all the studied samples being pure. The room temperature X-ray diffraction patterns of $La_2Mo_{1399}P_{0.01}O_{8.995}$ and

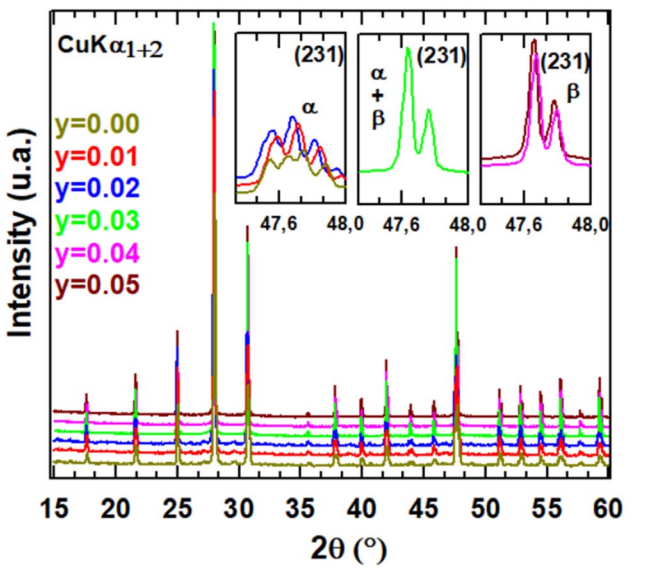

Fig. 1 Room temperature XRD patterns for different compositions of $La_2Mo_{2-y}P_yO_{9-y/2}$ series. The insets show the disappearance of the monoclinic splitting upon phosphorus substitution through the evolution of the (231) pseudocubic lines.

$La_2Mo_{1.98}P_{0.02}O_{8.99}$ clearly exhibit the pic splitting characteristic of the slight monoclinic distortion and the 2 × 3 × 4 superstructure peaks at low 2θ scattering angles relative to the β-$La_2Mo_2O_9$ form. This was confirmed by DT analysis in Fig. 2: an endothermic peak upon heating up associated with the reversible α → β structural phase transition was seen around 550–570 °C. With increasing phosphorus content, a slight shift of this transition toward higher temperatures is observed (Table 1). The reduction in the intensity of the thermal peak upon substitution is consistent with the slightly smaller monoclinic split-ting of the pseudocubic (231) diffraction line. The broadening of the peak (an increase of the difference between the temperature at the onset point and at the maximum peak in Table 1) reflects the increase of cationic disorder introduced by the phosphorus substitution.

A DTA analysis has been performed on $La_2Mo_{1.98}P_{0.02}O_{8.99}$ in order to detect the influence of phosphorus substitution on the α/β phase transition. The main effect is a significant decrease of the phase transition of about 45 °C relative to $La_2Mo_2O_9$: 580 °C for $La_2Mo_2O_9$ and about 536 °C for $La_2Mo_{1.98}P_{0.02}O_{8.99}$.

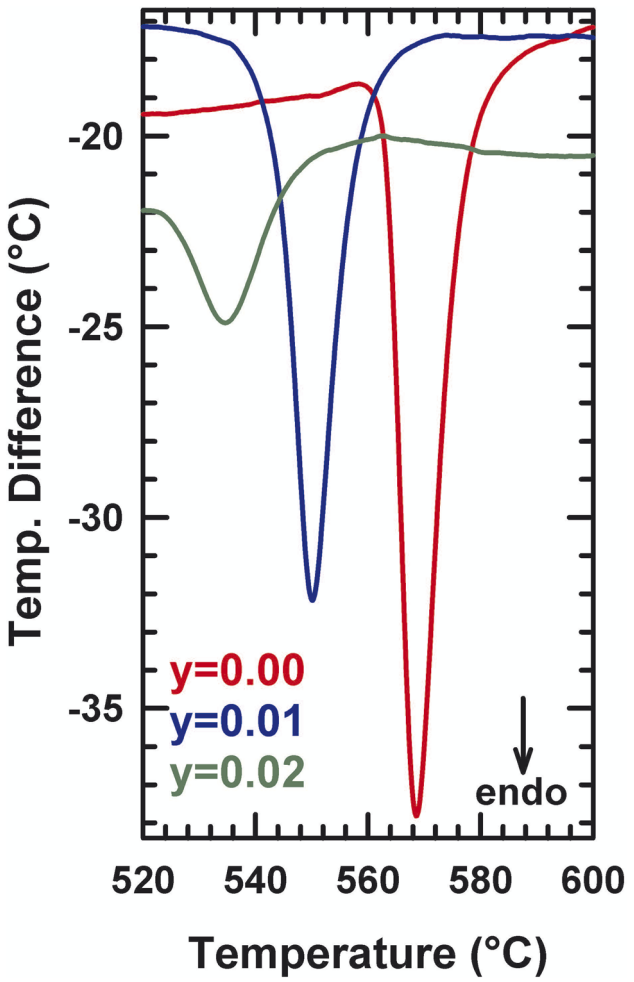

Fig. 2 DTA thermograms upon heating (10 °C min^{-1}) in air of $La_2Mo_{2-y}P_yO_{9-y/2}$ raw powders samples.

Table 1 First-order transition temperatures of raw powder of $La_2Mo_{2-y}P_yO_{9-y/2}$ determined by DTA in air

α → β transition temperature (°C)		
y	Onset	Peak max
0.0	568	570
0.01	549	551
0.02	533	536

This is consistent with the slightly smaller monoclinic splitting (see above) and the general trend of the β-phase stabilization upon substitution (see below). The thermal peaks upon heating and cooling are broader than those in $La_2Mo_2O_9$, probably due to some heterogeneity in the substitution as already evoked in another phase transition of the system. Above a phosphorus content of $y = 0.03$, the stabilization of the cubic β-phase at room temperature occurs. Table 2 musters the results of these structural refinements: atomic positions, equivalent isotropic temperature factors, and anisotropic thermal stirring coefficient.

3.2. Electrical properties

Observations on the electrical conductivity of specimens with varying phosphorous contents (Fig. 3) are helpful for describing polymorphism and studying the impact of the additive on the transport mechanism. To figure out the effect of the substituted amounts on the conduction mechanism, both Arrhenius and VTF (Vogel–Tammann–Fulcher) regimes are investigated. In the

Table 2 Refined crystal structure parameters (space group $P2_13$) in the series $La_2Mo_{2-y}P_yO_{9-y/2}$ from X-ray powder diffraction data

x		0.03	0.04	0.05
a (Å)		7.1525 (1)	7.1514 (1)	7.1494 (7)
La (4a) (*xxx*)	*x*	0.8546 (4)	0.8542 (7)	0.8551 (1)
	Occupancy	1	1	1
	B_{iso} ($Å^2$)[a]	4.7 (2)	4.1 (9)	4.6 (7)
Mo/P (4a)	*x*	0.1695 (7)	0.1716 (8)	0.1674 (4)
	Occupancy	0.985/0.015	0.980/0.02	0.975/0.025
	B_{iso} ($Å^2$)[a]	5.4 (4)	5.4 (1)	5.8 (5)
O1 (4a)	*x*	0.314 (8)	0.317 (3)	0.310 (9)
	Occupancy	1	1	1
	B_{iso} ($Å^2$)[a]	7	7	7
O2 (12b) (*xyz*)	*x*	0.987 (2)	0.960 (2)	0.969 (3)
	y	0.148 (5)	0.142 (9)	0.200 (5)
	z	0.360 (2)	0.350 (1)	0.347 (4)
	Occupancy	0.65 (7)	0.63 (7)	0.64 (7)
	B_{iso} ($Å^2$)[a]	7	7	7
O3 (12b)	x	0.796 (5)	0.780 (9)	0.822 (3)
	y	0.534 (5)	0.565 (5)	0.563 (5)
	z	0.599 (1)	0.624 (4)	0.576 (1)
	Occupancy	0.50 (3)	0.52 (3)	0.51 (3)
	B_{iso} ($Å^2$)[a]	7	7	7
R_{wp} (%)		8.60	7.78	9.97
R_{exp} (%)		4.52	5.33	6.05
R_{Bragg} (%)		3.35	2.34	3.21

[a] $B_{iso} = 4/3a^2(\beta_{11} + \beta_{22} + \beta_{33})$.

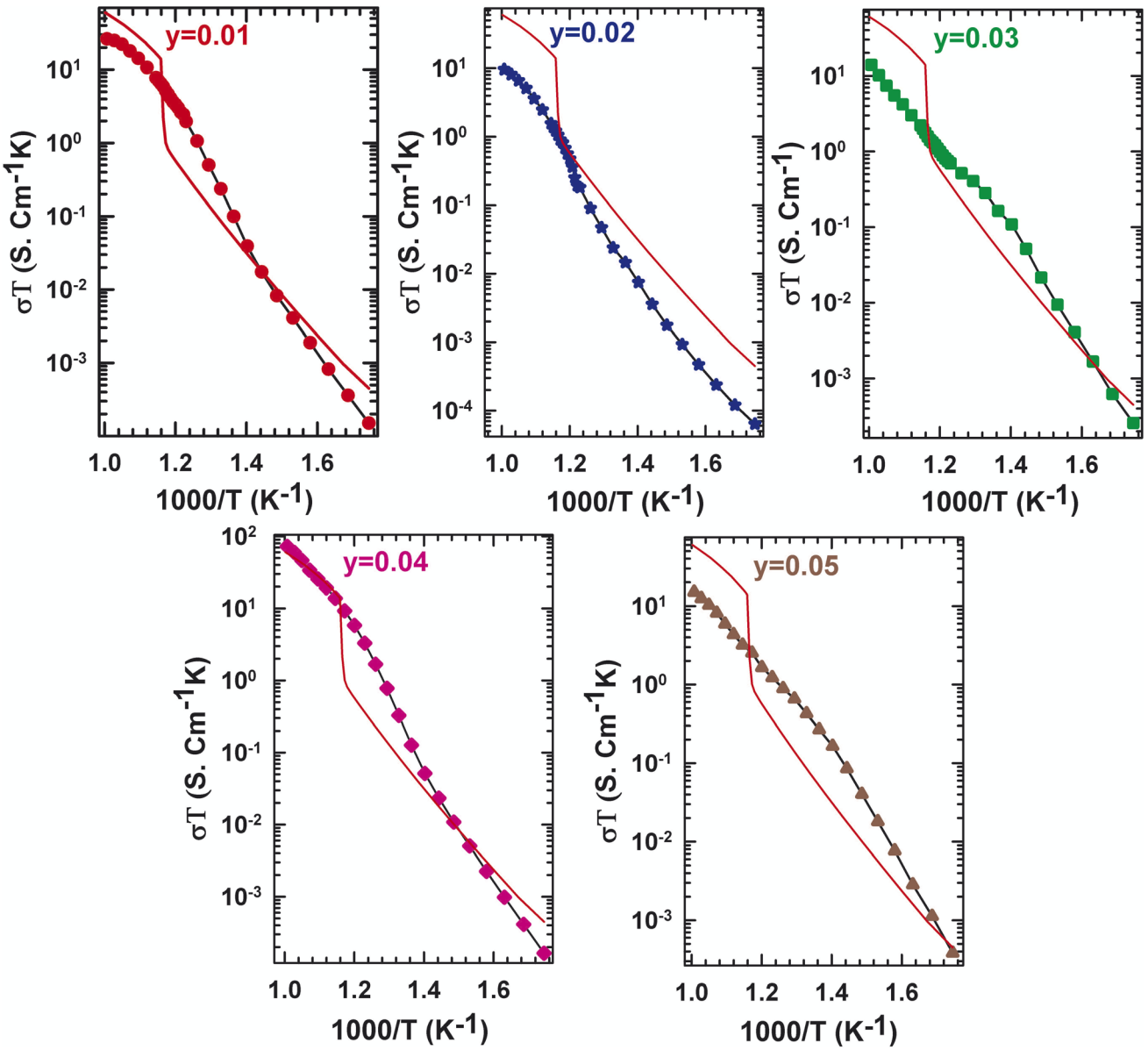

Fig. 3 Evolution of the conductivity with temperature for $La_2Mo_{2-y}P_yO_{9-y/2}$ ($y = 0$, 0.01, 0.02, 0.03, 0.04, 0.05).

low-temperature zone, the electric field of the samples is linear and follows the well-known Arrhenius law (eqn (1)):

$$(\sigma \times T) = \sigma_0 \exp(-\Delta E_a/k_B T) \quad (1)$$

where σ_0, E_a and k_B are the pre-exponential factor, the activation energy, and the Boltzmann constant, respectively. For assessing the electrical conductance of LAMOX materials in the high-temperature phase with inhibited phase transition, Georges *et al.* were the first to employ the Vogel–Tammann–Fulcher rule (eqn (2)).[27,28]

$$\left(\sigma \times \sqrt{T}\right) = \sigma_0 \exp[-\Delta K_B/R(T - T_0)] \quad (2)$$

where R and T_0 are resistance and glass transition temperature at equilibrium, respectively.

The two stages' boundaries are thought to be marked by a phase transition in a specific temperature. In this case, some results from Fig. 3, in which the plot of the dependence of the electrical conductivity of $La_2Mo_{2-y}P_yO_{9-y/2}$ samples, and the curve of the undoped $La_2Mo_2O_9$ was made for comparison, can be extracted. At 580 °C, the parent compound with $y = 0$ showed a phase transition, which can be seen by a sudden rise in conduction. Nevertheless, as the phosphorus level increases to $y = 0.05$, the phase transition that was previously described blurs and the conductivity jump disappears. The conductivity behavior of $y = 0.01$ and $y = 0.02$ does not exhibit an abrupt change at the transition temperature determined through DTA analysis and X-ray diffraction. This implies that pellets with $y = 0.01$ and $y = 0.02$ possess cubic symmetry throughout the thermal area examined. The stabilization of shape by

pressure within a sintered pellet has already been underlined for numerous members of the LAMOX family: $La_{1.8}Eu_{0.2}Mo_2O_9$ (ref. 24) et $La_{1.92}Ca_{0.08}Mo_2O_{8.96}$.[28] The experimentally observed decrease in the $La_2Mo_{2-y}P_yO_{9-y/2}$ series in oxide ion conductivity at a given temperature is very erratic depending on the y content. What's happened is most likely due to oxygen vacancy entrapment in such defect clusters.[27,29]

3.3. Spectroscopic properties

In order to track the dynamic properties of the system as a function of temperature and to better understand the transition mechanism, the Raman spectrometry study of LAMOX compounds was undertaken. Raman spectra of $La_2Mo_{2-y}P_yO_{9-y/2}$ (y = 0.01, 0.02, 0.03, 0.04, 0.05) were recorded in the frequency range 400–4000 cm^{-1}, as observed in Fig. 4. The first eye-catching in the figure is the resulting change in the spectrum profile at 840 cm^{-1} when $y \geq 0.03$ *P*-substituted. It's caused, therefore, by the transition from one phase α to another β, and confirms X-ray diffraction results. The characteristic vibration bands of PO_4^{3-} are listed in Table 3: the asymmetric (ν_3) and symmetric (ν_1) elongation of the P–O bands are 1017 and 938 cm^{-1}, respectively. Whereas, the asymmetric (ν_4) and symmetric (ν_2) deformation of the O–P–O bands are 567 and 420 cm^{-1}, respectively. Peaks that are registered below 200 cm^{-1} tend to be lattice structure modes. The measurement results in Fig. 4 shows a weak shift to the lowest values of wavenumbers, this would match with the change that occurred in the whole structure (decrease in overall volume, phase changeover, *etc.*). Additionally, the internal vibrational modes of a tetrahedral MoO_4 group of the specific original compound with $y = 0$ are explicated with details in literature[18]. Moreover, to supplement the XRD data, IR absorption was investigated. Some characteristic absorption bands are relative to PO_4^{-3} can be found in the spectra presented in Fig. 5. The two bands detected at 542 and 615 cm^{-1} correspond to the asymmetric bending (ν_4). While the asymmetric elongation is revealed by: the narrowband centered at 1015 cm^{-1} and the band observed at around 1050 cm^{-1}. Those spectroscopic bands and peaks are important and didactic since a change in shape can disclose information about the structure and phase transition.

Table 3 Characteristic band and vibration mode of PO_4^{3-} in Raman spectroscopy

Wavenumber	Vibration mode	Vibration pattern
1017	ν_3	Asymmetric elongation of P–O
938	ν_1	Symmetric elongation of P–O
567	ν_4	Asymmetric deformation of O–P–O
420	ν_2	Symmetric deformation of O–P–O

3.4. Thermal expansion

The thermal expansion behaviour of a solid electrolyte is also essential. The thermal expansion coefficient of $La_2Mo_2O_9$ is 14.1–16.0 × 10^{-6} K^{-1} at low temperature (α-$La_2Mo_2O_9$) and 16.4–22.5 × 10^{-6} K^{-1} at high temperature (β-$La_2Mo_2O_9$).[30,31] These values are much higher than those of YSZ and other oxide ion conductors (9–11 × 10^{-6} K^{-1}).[32] The relatively large thermal expansion is considered to be caused by the disordering of the oxygen lattice and minor oxygen loss during heating. It remains a hindrance for the compatibility of $La_2Mo_2O_9$ with common electrodes. It has been observed that the substitution of La and Mo sites of $La_2Mo_2O_9$ by various alkali and alkaline ions stabilizes the β phase at room temperature and increases the ionic conductivity and also reduces the thermal expansion coefficient.[33–35] Fig. 6 depicts the thermal development of the various compositions over the temperature range of $T_{ambiante}$ – 900 °C. It ought to be noted to mention that the sample with y = 0.02 behaves with a jump in the temperature

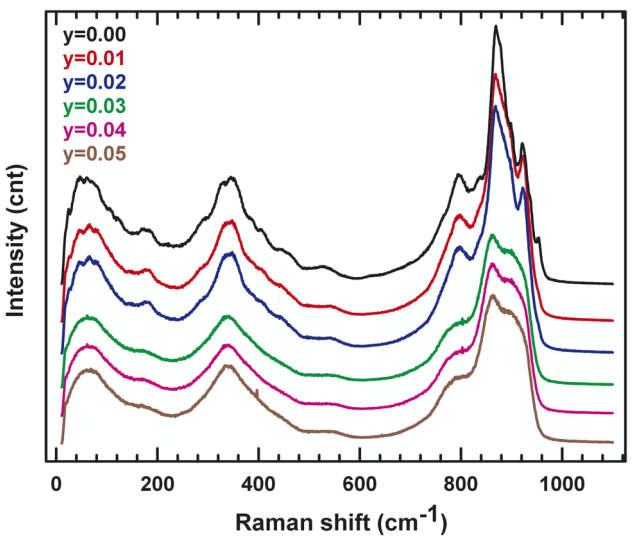

Fig. 4 Raman spectra of $La_2Mo_{2-y}P_yO_{9-y/2}$ (y = 0.01, 0.02, 0.03, 0.04, 0.05).

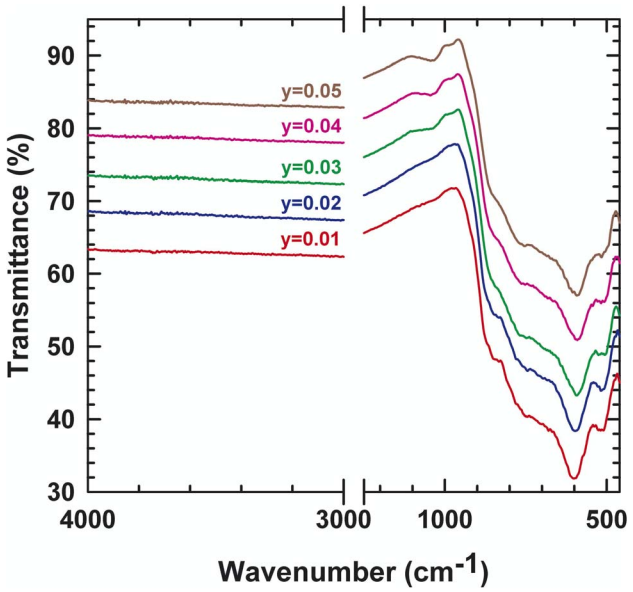

Fig. 5 IR spectra of $La_2Mo_{2-y}P_yO_{9-y/2}$ (y = 0.01, 0.02, 0.03, 0.04, 0.05).

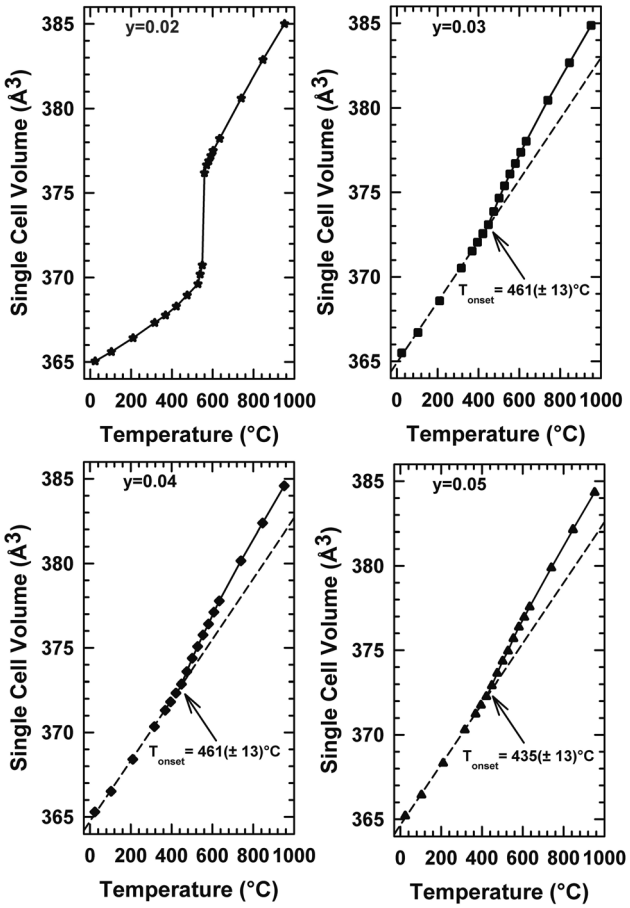

Fig. 6 Temperature dependencies of the single cell volume of $La_2Mo_{2-y}P_yO_{9-y/2}$ raw powder samples determined from temperature-controlled X-ray diffraction data.

range between 540 °C in the thermal evolution of cell volume. This behavior is associated with a clear deviation from the Arrhenius behavior in the conductivity curve. This alteration may be the result of the cationic framework distortion/liberation without symmetry breaking (Arrhenius to Vogel–Tammann–Fulcher (VTF) processes) moving from static to the dynamic disordering of oxygen vacancies. For compositions $y = 0.03$, $y = 0.04$, and $y = 0.05$, the volume increases linearly with the temperature up to about 400 °C, a temperature T_{onset} above which a change of speed is observed. The thermal changes in volume presented in Fig. 6 represent the LAMOX family's compound forms. In addition, the suppression of phase transition was confirmed in these three compositions and it supports our earlier DTA results.

4. Conclusion

A new examination of the solid solution $La_2Mo_{2-y}P_yO_{9-y/2}$ ($0.01 \leq y \leq 0.05$) was conducted to gain an improved grasp of the impact of pentavalent phosphorus on the crystal structure, thermal stability, electrical, and spectroscopic properties. Rietveld refinements of the XRD patterns demonstrate that the partial substitution of *P* at the Mo-site display the presence of three phases. The monoclinic system is adopted by the concentration less than or equal to 0.02. Whereas, a quasi-cubic phase has been observed at the content of 0.03. And, the cubic phase starts to appear from the $y = 0.04$ content of the phosphor. The stabilization of the cubic β-form is confirmed by the thermal expansion in which the sudden jump pronounced at $y = 0.02$, vanishes in the higher proportions. Thermal analysis reveals the disappearance of the phase transition, detected at 560 °C in $La_2Mo_2O_9$, from $y = 0.03$ to $y = 0.05$. Moreover, electrical conductivity measurements prove that the P doping could suppress the order-disorder transition exhibited by pure $La_2Mo_2O_9$, at room temperature from $y > 0.02$. An erratic decrease in conductivity as P content increases may be due to the fact of the oxygen vacancy. Infrared and Raman spectroscopies were commonly employed in the vibrational investigation. They point to the existence of the distinctive lines of molybdate ions and offer experimental proof of the function of phosphate ions.

Author contributions

Noureddine Mhadhbi: formal analysis, writing – original draft, data curation; Wiem Jabeur: writing, investigation, validation; Ahlem Guesmi: review & editing, visualization; Ammar Houas: methodology, resources; Naoufel Ben Hamadi: project administration; Houcine Naïli: methodology, validation, supervision.

Conflicts of interest

The authors declare no competing financial interest.

Acknowledgements

This work was supported and funded by the Deanship of Scientific Research at Imam Mohammad Ibn Saud Islamic University (IMSIU) (grant number IMSIU-RP23011).

References

1 D. J. L. Brett, A. Atkinson, N. P. Brandon and S. J. Skinner, Intermediate temperature solid oxide fuel cells, *Chem. Soc. Rev.*, 2008, **37**, 1568–1578, DOI: **10.1039/B612060C**.
2 E. D. Wachsman and K. T. Lee, Lowering the temperature of solid oxide fuel cells, *Science*, 2011, **334**, 935–939, DOI: **10.1126/science.1204090**.
3 N. Q. Minh and T. Takahashi, *Science and Technology of Ceramic Fuel Cells*, Elsevier Science, Amsterdam, Netherlands, 1995, pp. 1–15.
4 P. Lacorre, F. Goutenoire, O. Bohnke, R. Retoux and Y. Lallgant, Designing fast oxide-ion conductors based on $La_2Mo_2O_9$, *Nature*, 2000, **404**, 856–858, DOI: **10.1038/35009069**.
5 F. Goutenoire, O. Isnard, R. Retoux and P. Lacorre, Crystal structure of $La_2Mo_2O_9$, a new fast oxide-ion conductor, *Chem. Mater.*, 2000, **12**, 2575–2580, DOI: **10.1021/CM991199L/ASSET/IMAGES/LARGE/CM991199LF00008.JPEG**.

6 J. C. Lo, D. S. Tsai, Y. C. Chen, M. V. Le, W. H. Chung and F. J. Liu, $La_2Mo_2O_9$-based electrolyte: ion conductivity and anode-supported cell under single chamber conditions, *J. Am. Ceram. Soc.*, 2011, **94**, 806–811, DOI: 10.1111/J.1551-2916.2010.04168.X.

7 L. Malavasi, H. J. Kim, S. J. L. Billinge, T. Proffen, C. Tealdi and G. Flor, Nature of the monoclinic to cubic phase transition in the fast oxygen ion conductor $La_2Mo_2O_9$ (LAMOX), *J. Am. Chem. Soc.*, 2007, **129**, 6903–6907, DOI: 10.1021/JA071281E/ASSET/IMAGES/LARGE/JA071281EF00004.JPEG.

8 V. Voronkova, E. Kharitonova and A. Krasilnikova, Phase transitions and electrical conductivity of Bi-doped $La_2Mo_2O_9$ oxide ion conductors, *Phys. Status Solidi.*, 2009, **206**, 2564–2568, DOI: 10.1002/PSSA.200925184.

9 I. R. Evans, J. A. K. Howard and J. S. O. Evans, The crystal structure of α-La_2 Mo_2O_9 and the structural origin of the oxide ion migration pathway, *Chem. Mater.*, 2005, **17**(16), 4074–4077, DOI: 10.1021/cm050049%2B.

10 S. Georges, F. Goutenoire, O. Bohnke, M. C. Steil, S. J. Skinner, H.-D. Wiemhöfer and P. Lacorre, The LAMOX family of fast oxide-ion conductors: overview and recent results, *J. New Mater. Electrochem. Syst.*, 2004, **7**, 51–57, https://www.academia.edu/download/42653329/TheLAMOXFamilyofFastOxideIonConductors20160213-4521-11e6n6i.pdf.

11 S. Georges, F. Goutenoire, F. Altorfer, D. Sheptyakov, F. Fauth, E. Suard and P. Lacorre, Thermal, structural and transport properties of the fast oxide-ion conductors $La_{2-x}R_xMo_2O_9$ (R = Nd, Gd, Y), *Solid State Ionics*, 2003, **161**, 231–241, DOI: 10.1016/S0167-2738(03)00279-0.

12 Q. F. Fang, X. P. Wang, G. G. Zhang and Z. G. Yi, Damping mechanism in the novel $La_2Mo_2O_9$ based oxide ion conductors, *J. Alloys Compd.*, 2003, **355**, 177–182, DOI: 10.1016/S0925-8388(03)00278-0.

13 G. Corbel, E. Chevereau, S. Kodjikian and P. Lacorre, Topological metastability and oxide ionic conduction in $La_{2-x}Eu_xMo_2O_9$, *Inorg. Chem.*, 2007, **46**, 6395–6404, DOI: 10.1021/IC700876D/SUPPL_FILE/IC700876D-FILE015.PDF.

14 F. Goutenoire, O. Isnard, E. Suard, O. Bohnke, Y. Laligant, R. Retoux and P. Lacorre, Structural and transport characteristics of the LAMOX family of fast oxide-ion conductors, based on lanthanum molybdenum oxide $La_2Mo_2O_9$Basis of a presentation given at materials discussion No. 3, 26–29 September, 2000, University of Cambridge, UK, *J. Mater. Chem.*, 2001, **11**, 119–124, DOI: 10.1039/B002962I.

15 R. Subasri, D. Matusch, H. Näfe and F. Aldinger, Synthesis and characterization of $(La_{1-x}M_x)_2Mo_2O_{9-\delta}$; M=$Ca^{2+}$, Sr^{2+} or Ba^{2+}, *J. Eur. Ceram. Soc.*, 2004, **24**, 129–137, DOI: 10.1016/S0955-2219(03)00123-7.

16 I. Evans, J. Howard and J. Evans, The crystal structure of α-$La_2Mo_2O_9$ and the structural origin of the oxide ion migration pathway, *Chem. Mater.*, 2005, **17**(16), 4074–4077, DOI: 10.1021/cm050049%2B.

17 D. Marrero-López, J. Canales-Vázquez, J. C. Ruiz-Morales, J. T. S. Irvine and P. Núñez, Electrical conductivity and redox stability of $La_2Mo_{2-x}W_xO_9$ materials, *Electrochim. Acta*, 2005, **50**, 4385–4395, DOI: 10.1016/J.ELECTACTA.2005.02.002.

18 W. Jabeur, N. Mhadhbi, N. Ben Hamadi, A. Guesmi, T. Soltani and H. Naïli, Effect of humidified atmosphere on the physicochemical properties of S-doped $La_2Mo_2O_9$ oxide-ion conductors, *J. Mater. Sci. Mater. Electron.*, 2023, **34**, 1–13, DOI: 10.1007/S10854-022-09461-6/FIGURES/10.

19 R. D. Bayliss, S. N. Cook, S. Kotsantonis, R. J. Chater and J. A. Kilner, Oxygen ion diffusion and surface exchange properties of the α- and δ-phases of Bi_2O_3, *Adv. Energy Mater.*, 2014, **4**, 1301575, DOI: 10.1002/AENM.201301575.

20 J. A. Kilner and M. Burriel, Materials for intermediate-temperature solid-oxide fuel cells, *Annu. Rev. Mater. Res.*, 2014, **44**, 365–393, DOI: 10.1146/ANNUREV-MATSCI-070813-113426.

21 L. Malavasi, C. A. J. Fisher and M. S. Islam, Oxide-ion and proton conducting electrolyte materials for clean energy applications: structural and mechanistic features, *Chem. Soc. Rev.*, 2010, **39**, 4370–4387, DOI: 10.1039/B915141A.

22 A. Tarancón, Strategies for lowering solid oxide fuel cells operating temperature, *Energies*, 2009, **2**, 1130–1150, DOI: 10.3390/EN20401130.

23 M. Guzik, M. Bieza, E. Tomaszewicz, Y. Guyot, E. Zych and G. Boulon, Nd^{3+} dopant influence on the structural and spectroscopic properties of microcrystalline $La_2Mo_2O_9$ molybdate, *Opt. Mater.*, 2015, **41**, 21–31, DOI: 10.1016/J.OPTMAT.2014.11.013.

24 T. Matsumoto, K. Sunada, T. Nagai, T. Isobe, S. Matsushita, H. Ishiguro and A. Nakajima, Preparation of hydrophobic $La_2Mo_2O_9$ ceramics with antibacterial and antiviral properties, *J. Hazard. Mater.*, 2019, **378**, 120610, DOI: 10.1016/J.JHAZMAT.2019.05.003.

25 B. Pahari, N. Mhadhbi, G. Corbel, P. Lacorre and J. Dittmer, Analysis of the local structure of phosphorus-substituted LAMOX oxide ion conductors, *Dalton Trans.*, 2012, **41**, 5696–5703, DOI: 10.1039/c2dt12389d.

26 W. T. Pennington, IUCr, DIAMOND – visual crystal structure information system, *J. Appl. Crystallogr.*, 1999, **32**, 1028–1029, DOI: 10.1107/S0021889899011486.

27 G. Corbel, P. Durand and P. Lacorre, Comprehensive survey of Nd^{3+} substitution In $La_2Mo_2O_9$ oxide-ion conductor, *J. Solid State Chem.*, 2009, **182**, 1009–1016, DOI: 10.1016/J.JSSC.2009.01.016.

28 A. Selmi, G. Corbel and P. Lacorre, Evidence of metastability and demixion/recombination process in fast oxide-ion conductor $La_{1.92}Ca_{0.08}Mo_2O_{8.96}$, *Solid State Ionics*, 2006, **177**, 3051–3055, DOI: 10.1016/J.SSI.2006.07.050.

29 S. Basu, P. S. Devi and H. S. Maiti, Nb-Doped $La_2Mo_2O_9$: a new material with high ionic conductivity, *J. Electrochem. Soc.*, 2005, **152**, A2143, DOI: 10.1149/1.2047507.

30 T. Xia, J. Y. Li, X. Luo, Q. Li, J. Meng and X. Q. Cao, Electrical properties and dilatometric measurements of $La_2Mo_2O_9$ under low oxygen partial pressure, *Chin. J. Chem.*, 2005, **23**(6), 703–708, DOI: 10.1002/cjoc.200590703.

31 I. P. Marozau, A. L. Shaula, V. V. Kharton, N. P. Vyshatko, A. P. Viskup, J. R. Frade and F. M. B. Marques, Transport

properties and thermal expansion of $La_2Mo_2O_9$-based solid electrolytes, *Mater. Res. Bull.*, 2005, **40**, 361–371, DOI: 10.1016/j.materresbull.2004.10.003.

32 V. V. Kharton, F. M. B. Marques and A. Atkinson, Transport properties and thermal expansion of $La_2Mo_2O_9$-based solid electrolytes, *Solid State Ionics*, 2004, **174**, 135–149, DOI: 10.1016/j.ssi.2004.06.015.

33 D. M. Zhang, Z. Zhuang, Y. X. Gao, X. P. Wang and Q. F. Fang, Electrical properties and microstructure of nanocrystalline $La_{2-x}A_xMo_2O_{9-\delta}$ (A = Ca, Sr, Ba, K) films, *Solid State Ionics*, 2010, **181**, 1510–1515, DOI: 10.1016/j.ssi.2010.08.020.

34 T. Paul and A. Ghosh, Conduction and relaxation mechanisms in bismuth doped $La_2Mo_2O_9$ ionic conductors, *J. Appl. Phys.*, 2013, **114**, 164101, DOI: 10.1063/1.4826077.

35 P. Pinet, J. Fouletier and S. Georges, Conductivity of reduced $La_2Mo_2O_9$ based oxides: the effect of tungsten substitution, *J. Appl. Phys.*, 2007, **42**, 935–942, DOI: 10.1016/j.materresbull.2006.08.012.